The Chemist
Journal of the American Institute of Chemists

Adsorption of Brilliant Blue Dye by Synthesized g-C_3N_4: Characterization and Adsorption Parameters Insight

Manal Muhi Murad[1,2], Ayad F. Alkaim[2*]

[1]*Department of Chemistry, Al-Qasim Green university, Iraq*
[2]*Department of Chemistry, College of Sciences for Girls, University of Babylon, Hilla, Iraq*
**Corresponding author (E-mail: alkaimayad@gmail.com)*

Abstract: Graphitic carbon nitride (g-C_3N_4) has emerged as a promising metal-free nanomaterial for wastewater treatment due to its unique structural, thermal, and surface characteristics. In this study, g-C_3N_4 was successfully synthesized from melamine and thoroughly characterized using XRD, FESEM, FTIR, and EDX techniques to confirm its crystalline structure and morphology, identify the substance, and analyze its elemental composition and distribution. The synthesized material was evaluated as an efficient nanoadsorbent for the removal of Brilliant Blue dye from aqueous solutions. A comprehensive batch adsorption investigation was conducted to examine the effects of key operational parameters, including initial dye concentration, adsorbent dosage, and temperature. The results revealed that an increase in weight (0.025-0.1 g) increased the percentage of removal by 30-76% and decreased the adsorption capacity by 2.620-1.538 mg/g. When studying the effect of concentration, it was found that with an increase in concentration (1, 2, 3, 4, and 5) mg/L, the percentage of removal decreased by 40.00-13.14%, while the adsorption capacity increased by 0.8-1.3 mg/g. When studying the effect of temperature at different temperatures (40, 25, and 15)°C, it was found that the best removal was at a temperature of 40°C, where the percentage of removal decreased by 67-23.61% with an increase in concentration of 1-5 mg/L, while the adsorption capacity increased by 0.8-1.46 mg/g. This indicates that the reaction is endothermic, and, based on the R^2 value (0.9598), it follows the Freundlich model. The adsorption behavior indicated that both surface chemistry and environmental conditions play critical roles in controlling removal efficiency. Overall, this study highlights the potential of g-C_3N_4 as a high-performance nanoadsorbent for the removal of dyes from wastewater and provides valuable insights for future applications in environmental purification.

Key Words: g-C_3N_4, Brilliant Blue dye, adsorption, wastewater treatment, adsorption isotherm

1. Introduction

Chemical pollutants play a major role in the accumulation of toxins in aquatic ecosystems and bio-magnify up the food chain, ultimately affecting higher-level consumers [1]. A significant portion of the population relies on these water sources for drinking, sanitation, and recreational activities. Moreover, contaminated waterways can interfere with ecosystems, harm aquatic organisms, and diminish both environmental quality and the aesthetic value of urban areas [2,3]. The detection of chemical residues in wastewater is a growing global issue, primarily driven by human waste, inadequate disposal methods, and discharges from production facilities. These residues can often survive wastewater treatment procedures, resulting in the pollution of both surface and groundwater as well as soil, which presents serious threats to ecological systems and human health [4,5]. The presence of these chemical contaminants and dyes in water sources, even in low concentrations, poses a significant risk to human health and ecosystems. It may lead to severe mutagenic, genotoxic, and other ecotoxicological consequences for humans, animals, and plants [6,7].

Brilliant Blue (BB) is an anionic synthetic dye characterized by its vibrant, bright blue color. It is widely used across various industries, including food products, beverages, pharmaceuticals, and cosmetics. Also known as Brilliant Blue FCF, this dye features a triphenylmethane structure with the chemical composition: N-ethyl-N-(4-[(4-ethyl[(3-sulfophenyl)methyl]-amino]phenyl)(2 sulfophenyl)methylene]-2,5-cyclohexadien-1-ylidene)-3-sulfobenzene-methanaminium hydroxide inner salt, disodium salt, as shown in Figure 1(a) [8].

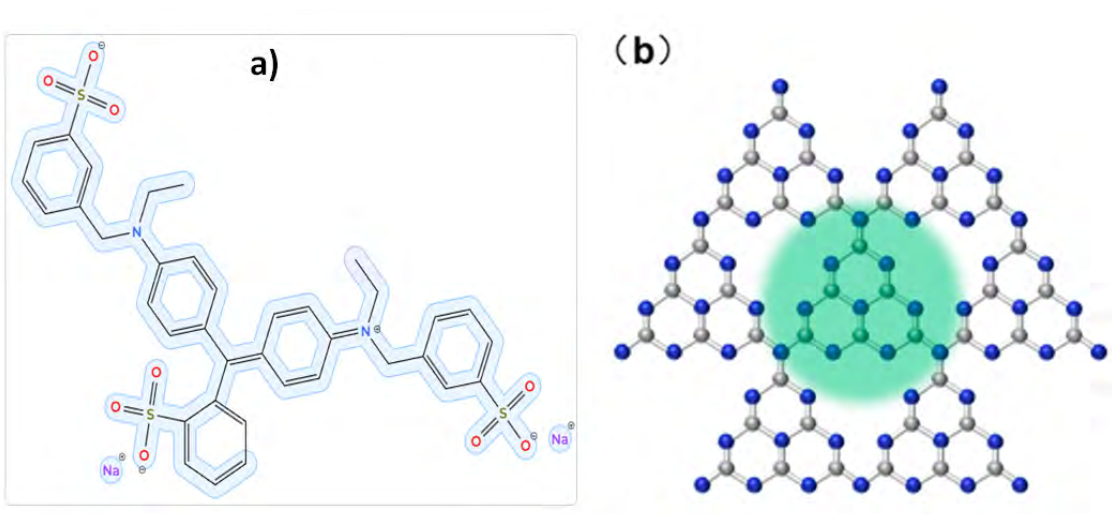

Fig 1. (a) Chemical Structure of Brilliant Blue (BB) Dye, (b) Chemical Structure of g-C_3N_4

Brilliant Blue, a widely used textile dye, persists as a non-degradable contaminant in aquatic environments. Its pronounced toxicity, vivid pigmentation, and resistance to standard treatment methods make it particularly hazardous to aquatic organisms, presenting significant ecological risks. To address this challenge, nanotechnology—particularly the use of quantum dots (QDs)—has shown considerable promise as an innovative approach to environmental remediation [9,10]. To remove these organic dyes and eliminate their toxicity, several traditional treatment methods have been developed, including electrochemical, co-agulation, ultrafiltration, photocatalysis, adsorption, and co-precipitation [11,12]. However, these techniques must be continually developed and refined to reduce operating costs [13,14]. Due to its cost-effectiveness, ease of operation, and high efficiency, the adsorption technique has become a widely adopted method for water purification [15,16]. Adsorption is a chemical and physical phenomenon that occurs as a result of forces present on the surface of a liquid or solid. Materials adhere to the surface due to these forces; as a result of a decrease in the system's free energy and entropy, adsorption occurs, a spontaneous process. Graphitic carbon nitride ($g\text{-}C_3N_4$), as shown in Figure 1(b), is a two-dimensional semiconductor polymer composed entirely of carbon and nitrogen, two of the most abundant elements on Earth, which together account for approximately 99% of the Earth's crust [17,18]. Graphitic carbon nitride ($g\text{-}C_3N_4$) exhibits exceptional physical and chemical properties, including robust chemical and thermal stability, cost-effectiveness, scalability, and environmental compatibility. These distinctive characteristics position $g\text{-}C_3N_4$ as a crucial material for addressing global environmental challenges through diverse applications, such as photocatalytic degradation of persistent dyes, pharmaceuticals, and pollutants; solar-driven hydrogen production; CO_2 reduction; nitrogen fixation; antimicrobial treatments; and advanced sensor technologies [19-21]. Nonetheless, pure $g\text{-}C_3N_4$ exhibits certain drawbacks, including limited visible-light response, a small surface area, and a low electron-hole separation rate. These negative aspects greatly diminish photocatalytic effectiveness [22,23].

The removal of dyes from aqueous solutions by adsorption is among the most effective techniques available. Consequently, adsorption methodologies facilitate the extraction of pigments from concentrated industrial effluents. Nevertheless, regenerating a significant proportion of adsorbents poses considerable challenges. Furthermore, the financial expenditure associated with adsorption processes utilizing such materials is substantial. In contemporary research, nanotechnology has emerged as one of the most noteworthy advancements for the effective removal of dyes from wastewater through adsorption. This technology demonstrates efficacy in treating water contaminated with trace amounts of organic and inorganic dyes and is more cost-effective than alternative methods. Recently, nanoparticles and nanocomposites have been identified as the most effective agents for both adsorption and photo-catalytic processes aimed at the complete removal of dyes from wastewater [24-27]. $G\text{-}C_3N_4$ is an organic semiconductor material with advantageous properties, including non-toxicity, reliability in terms of chemical resistance, and affordability [28].

In this study, a nanomaterial based on graphitic carbon nitride ($g\text{-}C_3N_4$) was synthesized from melamine, a precursor rich in carbon and nitrogen. The structural and morphological characteristics of the prepared nanomaterial were examined using XRD, SEM, FTIR, and EDX to elucidate its crystalline structure and surface morphology. The adsorption efficiency of $g\text{-}C_3N_4$ was subsequently evaluated for the removal of selected dye pollutants commonly found in wastewater, such as Brilliant Blue. By measuring the absorbance of the treated sample and calculating the corresponding removal percentages, the overall performance of g-C_3N_4 as an effective adsorbent for eliminating dyes contaminants from polluted water was assessed.

2. Materials and Methods

Melamine: chemical formula ($C_3H_6N_6$) with molecular weight 126 g/mole and its purity 99.8%, production company (Zhejiang Polymer Chemical Co., Ltd.); Brilliant Blue dye: chemical formula ($C_{37}H_{34}N_2Na_2O_9S_3$) with molecular weight 792.85 g/mole and its purity 85%; ethanol: chemical formula (C_2H_5OH) with molecular weight 46.07 g/mole and its purity 70% production company (JOUDTOL); distilled water.

Preparation of g-C_3N_4

One method for producing g-C_3N_4 powder involved the direct thermal treatment of nitrogen-rich organic precursors, such as melamine. Melamine was heated to 500°C for 4 hours in a muffle furnace within a covered alumina crucible [29]. Then, the material was pulverized using a mortar and pestle. By applying this treatment, we have synthesized g-C_3N_4. Then, g-C_3N_4 was washed by ethanol to get rid of impurities. The purity of the synthesized g-C_3N_4 was confirmed through XRD, SEM, FTIR, and EDX measurements for use in this study as a nanosurface in the adsorption process.

Adsorption Study

A stock solution of Brilliant Blue dye was prepared at a concentration of 50 mg/L, and from this, different concentrations (1 , 2, 3, 4, and 5) mg/L were prepared in order to study the effect of concentration on the adsorption process of the BB dye. Then the effect of temperature for the same concentrations was also studied at (15, 20, and 40)°C, as well as the effect of surface mass (g-C_3N_4) for weights (0.025, 0.05, 0.075, 0.1) g at 25°C, after studying each effect, the prepared solutions were first and second separated using a centrifuge, and then the absorbance of the solutions was measured at the wavelength of the Brilliant Blue dye (560 nm). The removal percentage and adsorption capacity were calculated for equations 1 & 2:

$$R\% = \frac{C_o - C_e}{C_o} \times 100 \qquad (1)$$

where C_o (mg/L) is the initial concentration of BB dye solution, C_e (mg/L) is the concentration of BB dye solution at equilibrium;

$$Q_e = \frac{(C_o - C_e)V}{W} \qquad (2)$$

where Q_e is the adsorption capacity at equilibrium (mg/g), C_o is the initial concentration of solution (mg/L), C_e is the concentration of solution at equilibrium (mg/L), V is the volume of solution (L or ml) , and W is the mass of adsorbent (g).

3. Results and Discussion

FESEM/EDX

Scanning electron microscopy (SEM) was employed to examine the surface morphology and microstructural features of the synthesized g-C_3N_4. As shown in Figure 2(a) and (b), the material exhibits a well-defined rod-like nanostructure with relatively uniform geometry.

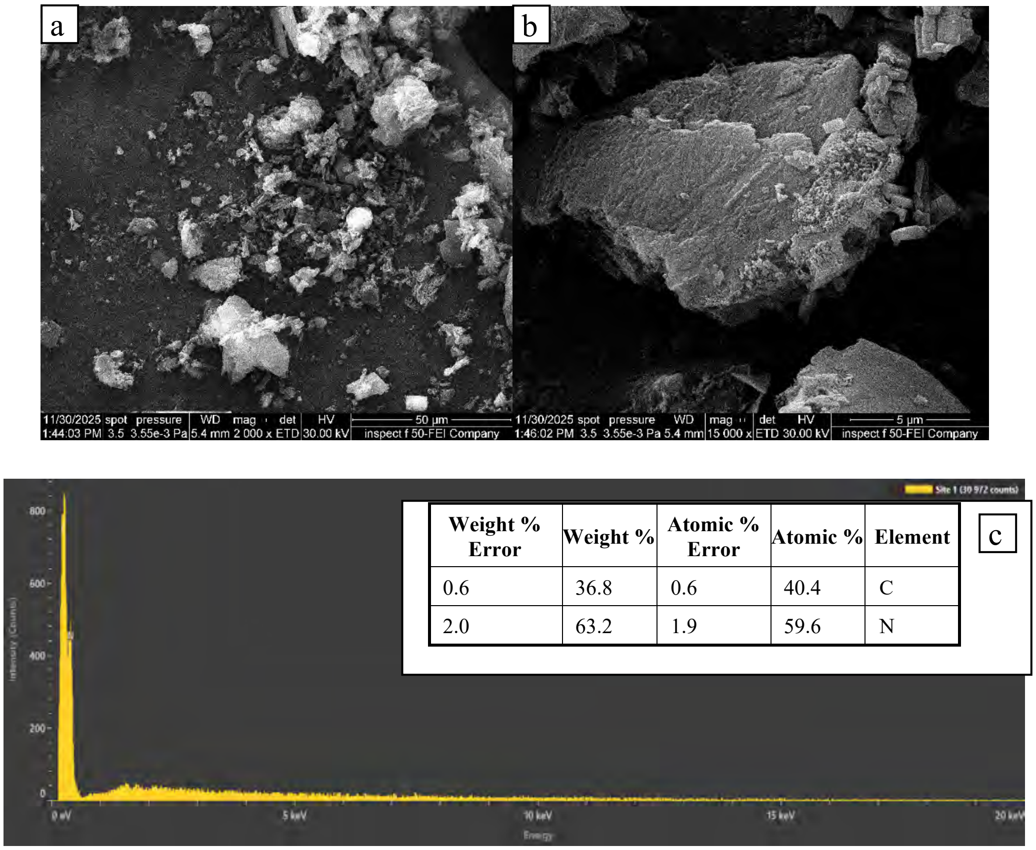

Weight % Error	Weight %	Atomic % Error	Atomic %	Element
0.6	36.8	0.6	40.4	C
2.0	63.2	1.9	59.6	N

Fig 2. (a-b) FESEM Image of g-C_3N_4 Nanoparticles, and (c) EDX of g-C_3N_4 Nanoparticles

The observed rods possess characteristic dimensions on the order of ~1.33 µm in length and ~50 µm in diameter, while the rod width is approximately 5 µm, indicating a highly anisotropic nanostructure. Notably, the surface of the g-C_3N_4 rods exhibits abundant nanoscale pores, cracks, and structural defects, contributing to a hierarchically porous architecture. These surface irregularities significantly increase the effective surface area and expose numerous accessible active sites [30,31]. The coexistence of mesopores and macropores, as evident in Figure 2(a) and (b), is particularly advantageous for adsorption-based wastewater treatment, as it minimizes mass-transfer resistance and facilitates rapid diffusion of organic pollutants and dye molecules from the aqueous phase to the internal adsorption sites. Overall, the rod-like morphology, combined with the porous surface texture, enhances adsorption efficiency by promoting pollutant accessibility, accelerating transport kinetics, and improving the interaction between contaminants and the reactive surface of g-C_3N_4. This microstructural design is therefore highly favorable for applications in wastewater remediation and adsorption-driven purification processes [32,33]. EDX is a method for recognizing elements within a sample. Various shapes like squares, lines, and small areas (dots) can be analyzed using EDX. It serves as a vital research tool to enhance the efficiency of manufacturing processes. The EDX analysis (Figure 2c) confirmed that the produced g-C_3N_4 consists of Carbon (C) and Nitrogen (N) [34,35].

X-Ray Diffraction (XRD)

The crystalline structure of the synthesized g-C_3N_4 was investigated using X-ray difffracttion (XRD), and the resulting diffraction pattern is presented in Figure 3.

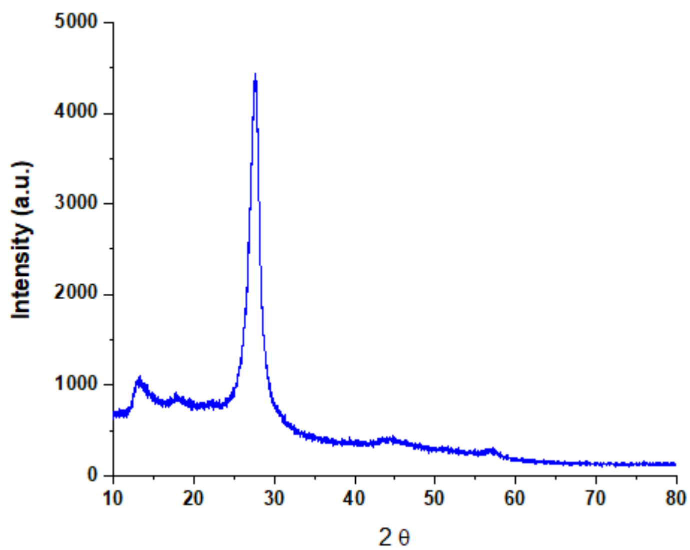

Fig 3. XRD of g-C_3N_4 Nanoparticles Surface

The diffractogram exhibits a dominant sharp diffraction peak centered at approximately 2θ ≈ 27.4°, which is characteristic of the (002) crystallographic plane of graphitic carbon nitride. This peak corresponds to the interlayer stacking of conjugated aromatic layers, reflecting the periodic arrangement of tri-s-triazine (heptazine) units along the c-axis [36,37].

A weaker and broader diffraction feature observed in the low-angle region around 2θ ≈ 13.0° can be attributed to the (100) in-plane structural packing of the heptazine units. The broad nature of this peak indicates limited long-range order within the in-plane framework, which is typical of polymeric g-C_3N_4 materials synthesized via thermal polycondensation.

The pronounced intensity and sharpness of the (002) peak suggest a relatively high degree of interlayer ordering, while the overall peak broadening reflects the nano-scale dimensions and partial structural disorder of the material. The absence of additional diffraction peaks confirms the phase purity of the synthesized g-C_3N_4, with no detectable crystalline impurities or secondary phases.

The reduced crystallinity combined with nanoscale structural disorder is advantageous for adsorption and photo-catalytic applications, as it introduces defect sites and enhances surface reactivity. These structural features are consistent with the SEM observations and enhance mass transport and active-site availability during pollutant adsorption or catalytic processes [38,39].

Fourier Transform Infrared (FTIR)

Analyzing the FTIR spectra allows for a clear understanding of functional group linkages. Figure 4(a) shows the Fourier transform infrared (FTIR) spectra of g-C_3N_4, and Figure 4(b) also shows the Fourier transform infrared (FTIR) spectra of g-C_3N_4 after the adsorption of the Brilliant Blue dye.

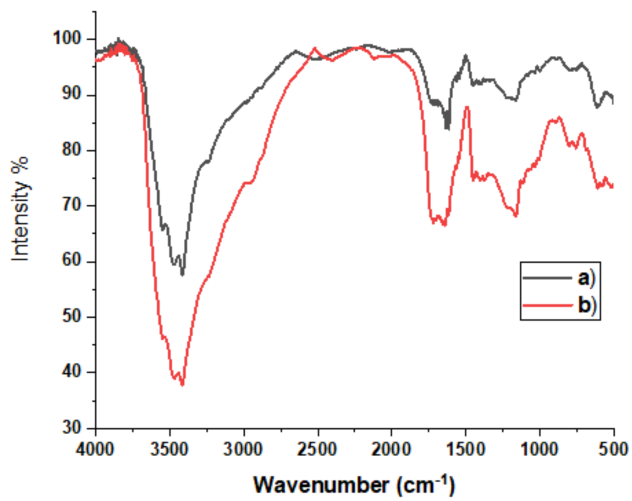

Fig 4. (a) FTIR for g-C3N4 Before Adsorption BB Dye, and (b) g-C3N4 After Adsorption BB Dye

Significant changes appeared in the Fourier transform infrared spectrum of the compound after the adsorption of Brilliant Blue dye. A slight shift in the N-H expansion band was observed, from 3090 cm^{-1} to 3080-3045 cm^{-1} [40,41]. This suggests possible interactions between the amine groups of the g-C_3N_4 surface and the sulfonate or aromatic groups of the dye molecules. Furthermore, more intense C=N, C-N bands were observed in the region between 1400-1600 cm^{-1}, possibly due to л - л stacking interactions between the aromatic rings of Brilliant Blue and the conjugated heptazine units of g-C_3N_4. Additional new peaks appeared at 1483, 1458, 1433, 1330, 1244, and 1209 cm^{-1} after adsorption. Overall, the appearance of new functional group vibrations, intensity changes, and spectral shifts indicates successful adsorption Brilliant Blue dye on the surface of g-C_3N_4 [42].

Adsorbent Dosage

One of the most important factors affecting the adsorption process is the weight of the adsorbent. Different amounts of g-C_3N_4 (0.025-0.1 g) on the adsorption of a dye (5 mg/L dye solution at pH 7), while keeping all other parameters constant, the solutions were shaken for 60 min at 25°C. Figure 5 shows that the amount of adsorbent material is directly related to the percentage removal, with higher pollutant uptake observed as the adsorbent dose increases.

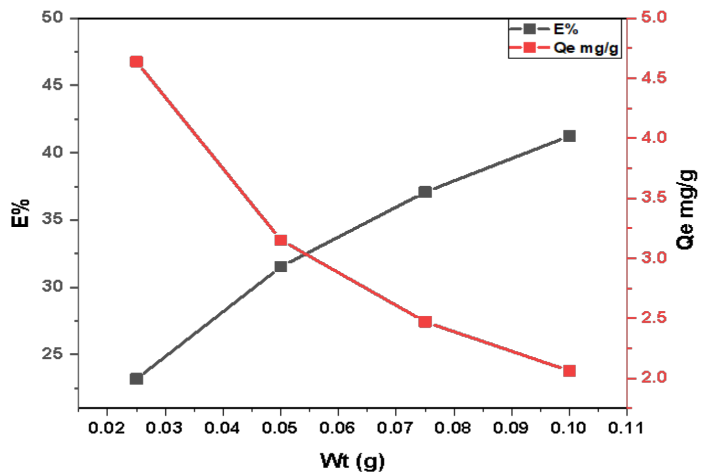

Fig 5. Effect of the Weight of g-C_3N_4 on the Removal of BB Dye

A higher adsorbent dose increases the number of active exchangeable sites on its surface, thereby facilitating ion capture. Furthermore, lower doses of adsorbents accelerate the adsorption rate due to the greater abundance of accessible active sites. Conversely, when a high adsorbent dose is used, dye ions may be unable to reach the adsorption sites until equilibrium is est-ablished. In general, increasing the adsor-bent dose can reduce the total solute adsorp-tion per unit mass of adsorbent due to interactions among the adsorbent's active sites.[1,38,43].

Effect of Concentration

Figure 6 shows solutions prepared at different concentrations (1-5) mg/L under the same conditions of weight (0.05 g) and temperature (25°C), where the adsorption capacity increases with increasing concentration and, therefore, the percentage of removal decreases with increasing concentration.

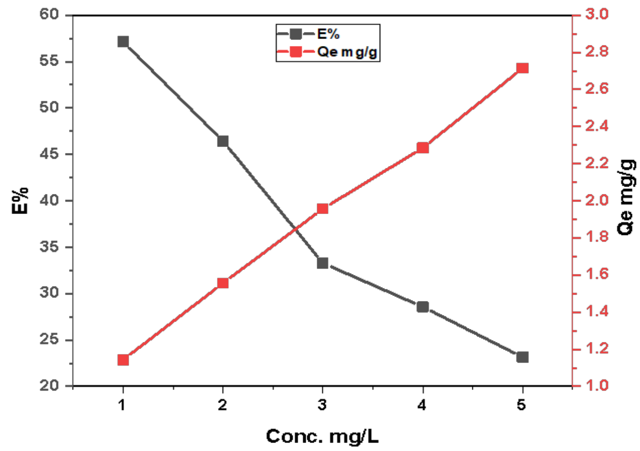

Fig 6. Effect of Concentration of BB Dye Solution on Adsorption Process

The dye molecules become more saturated with the adsorbent or surfaces, competing for the limited active sites, thus reducing the ability of the adsorbent or process to remove a greater percentage of the dye. The removal of dyes through sorption is closely related to their starting concentration [44,45]. This relationship is associated with the number of available active sites on the adsorbent and the concentration of dye molecules. In general, the initial dye concentration in water plays a crucial role as a driving force, facilitating mass transfer from the bulk solution to the adsorbent surface. Consequently, as the initial dye concentration increases, the driving forces also become stronger. Thus, in solutions with a high concentration of dye, the molecules encounter greater difficulty in locating binding sites on the adsorbent's surface [46,47].

Effect of Temperature

g-C_3N_4 was employed as a nanomaterial adsorbent for the treatment of contaminated dyes, specifically Brilliant Blue, under various temperature conditions (15, 25, and 40) °C and different concentrations of 1-5 mg/L of BB dye, as shown in Figure 7. The most effective adsorption was observed at 40°C.

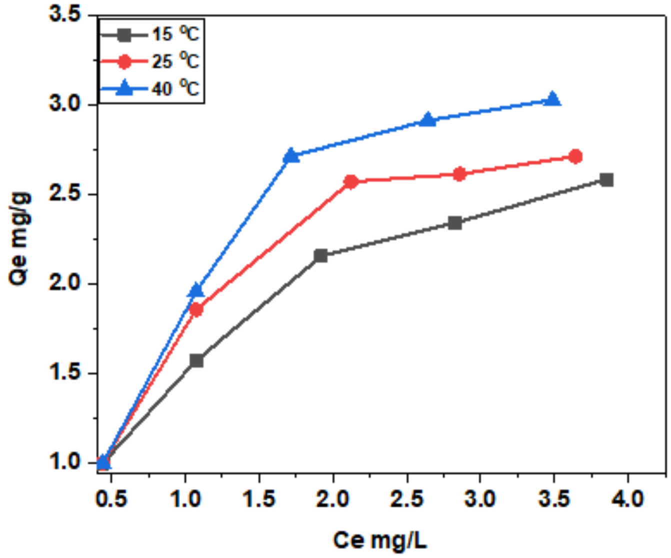

Fig 7. Temperature Effect on Adsorption of BB Dye

This is because raising the temperature provides the energy required for dye molecules to adhere to the g-C_3N_4 adsorbent surface. It is well known that physical adsorption is an endothermic process; as temperature rises, adsorption efficiency increases, leading to a higher removal percentage. Consequently, increasing the temperature increases the adsorption rate because the dye molecules have higher kinetic energy. This results in higher diffusion and adsorption rates, facilitating the establishment of equilibrium between the adsorbent, g-C_3N_4 , and the adsorbate, Brilliant Blue dye. Moreover, higher temperatures yielded optimal conditions for physical adsorption [48-50].

Thermodynamic Parameters

Thermodynamic analysis was performed to evaluate the feasibility and spontaneity of the sorption process. Key thermodynamic parameters, including the Gibbs free energy change (ΔG°), enthalpy change (ΔH°), and entropy change (ΔS°), were determined using the Van't Hoff approach [51]. The values of ΔH° and ΔS° were obtained from the slope and intercept of the linear plot of ln Kd versus 1/T (Figure 8), respectively, according to equation 3:

$$\ln K_d = \frac{\Delta S^\circ}{R} - \frac{\Delta H^\circ}{RT} \tag{3}$$

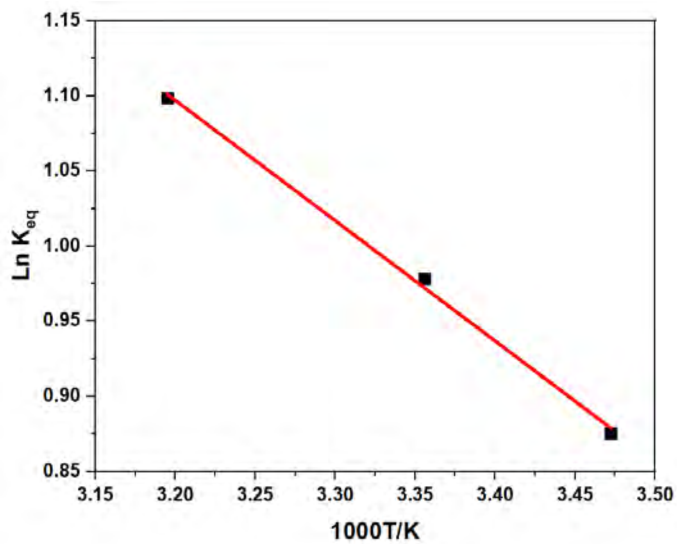

Fig 8. Van't Hoff's Plot on the Removal BB Dye onto g-C_3N_4 Nanoparticles

The thermodynamic parameters associated with adsorption from solutions offer significant insights into the nature and mechanism of the adsorption process. The standard Gibbs free energy change ΔG is computed as follows (equation 4):

$$\Delta G° = - RT \ln K \quad (4)$$

A negative Gibbs free energy indicates the viability and spontaneity of the adsorption process [52].

The thermodynamic factors presented in Table 1 provide essential insight into the nature of BB dye adsorption onto g-C_3N_4. The positive ΔH values confirm that the adsorption process is endothermic, consistent with the observed decrease in Q_{max} as temperature increases. Moreover, the magnitude of ΔH 6.666 kJ mol^{-1}) is well below 40 kJ mol^{-1}, indicating that the adsorption is dominated by physisorption, where reversible intermolecular forces govern the interaction between the dye molecules and the adsorbent surface [53,54].

Table 1. Thermodynamic Factors for the Adsorption of BB onto g-C_3N_4 Nanoparticles

T/K	*ΔG°* *(kJ.mol^{-1})*	*ΔH°* *(kJ.mol^{-1})*	*ΔS°* *(J.K^{-1}.mol^{-1})*
288	-0.8674	6.666	30.435
298	-0.647		
313	-0.366		

From the values of Free Gibbs Energy (ΔG°) in Table 1 for all temperatures (15, 25, 40) °C are negative (-0.867, -0.647, and -0.366) kJ/mol. Respectively, this means the adsorption process is spontaneous through this range of temperature [55].

A positive value of entropy ΔS° (30.435)kJ/K mol indicates increased randomness in (solid-liquid) adsorption systems due to structural changes in the surface of the adsorbent material during the process [49,56,57].

Adsorption isotherm

To assess the distribution of the adsorbate from the liquid phase to the solid phase until equilibrium is reached under controlled (constant) conditions, it is essential to utilize an instrument for studying adsorption isotherms [58,59]. In this research, the Langmuir and the Freundlich models were utilized to assess the adsorption properties. The Langmuir isotherm postulates that adsorption occurs in a monolayer on a surface with a limited number of uniform sites and that there is no interaction among the adsorbed molecules. It can be represented as (equation 5):

$$Q_e = \frac{q_m K_L C_e}{1+K_L C_e} \quad (5)$$

where q_e refers to the quantity of adsorbate that is adsorbed at equilibrium (mg /g), q_{max} signifies the maximum adsorption capacity achievable when monolayer coverage is complete (mg/g), C_e indicates the equilibrium concentration of the adsorbate present in solution (mg/L), and KL represents the Langmuir equilibrium constant, which is associated with the affinity for binding sites (L /mg) [3,60].

An empirical model that characterizes adsorption onto heterogeneous surfaces with a non-uniform distribution of adsorption heat is the Freundlich isotherm. Its equation is as follows (equation 6):

$$q_e = K_f C_e^{1/n} \quad (6)$$

The q_e is the amount of adsorbate adsorbed at equilibrium (mg/g), K_F is the Freundlich constant that indicates the adsorption capacity ($mg1^{-1}/n\ g^{-1}L1/n$), C_e is the equilibrium concentration of the adsorbate in solution (mg/L), and n is the heterogeneity factor (dimensionless), with values of $1 < n < 10$ indicating favorable adsorption [61,62].

The results in Table 2 indicate that the adsorption process occurred on a heterogeneous surface and may involve multilayer adsorption. The Freundlich model provides the best fit to the data ($R^2 = 0.9598$), indicating that the surface is heterogeneous and that adsorption occurs at sites with different energies. However, the Langmuir model also yielded good results ($R^2 = 0.9544$), as the difference between the two models is minimal.

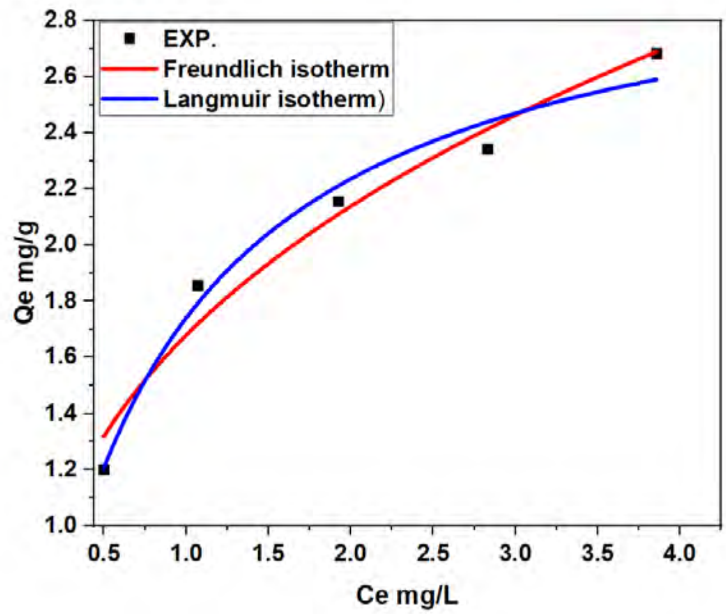

Fig 9. Adsorption Models Freundlich and Langmuir Isotherms

Figure 9 shows that the adsorption of Brilliant Blue dye best follows the Freundlich model. This indicates a heterogeneous distribution of adsorption sites on the adsorbent surface, as the increase in adsorption efficiency (Q_e) with increasing equilibrium concentration (C_e) reflects g-C_3N_4's efficiency in removing the dye at high concentrations [63,64].

Table 2. Adsorption Isotherm Models of the Freundlich and Langmuir

Nonlinear adsorption isotherm model		
Isotherm	**Parameter**	**Dye Temperature 25°C**
Freundlich	K_f	1.6.02 ± 0.044
	1/n	0.32 ± 0.022
	R^2	0.9598
Langmuir	q_m(mg/g)	2.88±0.023
	K_L(L/mg)	0.3111± 0.0113
	R^2	0.9544

4. Conclusion

The synthesized adsorbent exhibited an efficient adsorption performance toward the target pollutant, which can be attributed to its porous structure and the availability of abundant active sites that facilitate mass transfer and surface interactions. Adsorption experiments demonstrated that initial concentration, temperature, and adsorbent dose significantly influence the adsorption behavior, confirming the dominant role of electrostatic interactions and mediated effects. Thermodynamic analysis revealed negative ΔG° values, indicating that the adsorption process is spontaneous, while the positive ΔH° value confirmed its endothermic nature. The positive ΔS° further suggested increased randomness at the solid–solution interface during adsorption. Overall, the results confirm that the adsorption process is feasible and energetically favorable. These findings highlight the potential of the prepared material as an effective adsorbent for wastewater treatment and provide a useful basis for future optimization and practical applications. Based on the R^2 value (0.9598), the data follows the Freundlich model. The adsorption behavior indicated that both surface chemistry and environmental conditions play critical roles in controlling removal efficiency.

5. References

1. Hameed BH, El-Khaiary MI. Sorption kinetics and isotherm studies of a cationic dye using agricultural waste: broad bean peels. *J. Hazard. Mater.*, 2008, 145. 639-648.
2. Huan S. Identifying complex relationship in sub-fields between digital economy and urban ag-glomeration water pollution in Yangtze River Economic Belt: Evidence from original large-scale social media text analysis. *Chaos, Solitons Fractals*, 2025, 200, 117016.
3. Habila MA, Alothman ZA, Ali R, Ghafar AA, Hassouna MSE-D. Removal of tartrazine dye onto mixed-waste activated carbon: Kinetic and thermodynamic studies. *Clean: Soil, Air, Water*, 2014, 42(12), 1824-1831.
4. Mohd Hanafiah Z, Wan Mohtar WHM, Abdul Maulud KN, Wan-Mohtar WAAQI, Ebrahim MN, Binti Abd Manan TS, Indarto A, Afan HA, Yaseen ZM. Global pharmaceutical pollution in waterways: Insights from sewage treatment point sources. *Emerging Contam.*, 2025, 11(4), 100585.
5. Haghbin MR, Niknam Shahrak M, LotfiKatooli L, Mirzaei S. Potential of green-based microporous carbon for advanced water decontamination from azo dyes: Experiment and molecular dynamic simulation studies. *J. Env. Chem. Eng.*, 2024, 12(1), 111875.
6. Meenu O, Samuel EJJ. Can manganese-based ternary photocatalysts provide effective solutions for pharmaceutical pollution in aquatic environments? A comprehensive review. *Inorg. Chem. Commun.*, 2026, 183, 115641.
7. Mosaa ZA, Bader AT, Aljeboree AM, Alkaim AF. Adsorption and removal of textile dye (methylene blue mb) from aqueous solution by activated carbon as a model (apricot stone source waste) of plant role in environmental enhancement. *Plant Arch.*, 2019, 19, 910-914.
8. Sreelekshmi RC, Govindasamy M, Saraswathyamma B. Synergistic RuS_2/CeS_2 nano-hybrid for electrochemical detection of Brilliant Blue dye. *J. Food Eng.*, 2026, 403, 112731.

9. Azzam MM, Labib AA, Handal HT, Mousa HA, Galal HR, Ibrahem IA, Fawzy MM, Ahmed MAM, Rwayhah YMN, Mohamed WAA. Study of photophysical properties on recycling for solar and photo degradation process of Brilliant Blue R dye and real industrial wastewater using Bentonite/TiO_2 QDs. *Mater. Sci. Eng.: B*, 2025, 314, 117991.
10. Zhou Z, Lin S, Yue T, Lee T-C. Adsorption of food dyes from aqueous solution by glutaraldehyde cross-linked magnetic chitosan nanoparticles. *J. Food Eng.*, 2014, 126, 133-141.
11. Jamalabad GS, Mohagheghi MMB. Effect of GO and rGO on the photocatalytic and adsorption properties of $SnFe_2O_4$ for crystal violet dye removal. *Eur. Phys. J. Plus*, 2025, 140(11).
12. Egerić M, Petrović D, Vujasin R, Wu YN, Li F, Janolin PE, Matović L, Devečerski A. Enhanced adsorption–photocatalytic degradation of the Congo red dye in the presence of the MOF/activated carbon composite catalysts. *Water (Switz.)*, 2025, 17(24).
13. Akhtar MN, Ghaffar J, Sheikh TA, Raza MA, Michalczyk M, Zierkiewicz W, Latif S, Alshammari AQ, Alshammari A, Imran M, Aldamen MA, Ahmed M. Experimental and theoretical insight into the adsorption mechanism of organic dye by a paddle wheel type Cu(II) complex. *J. Mol. Struct.*, 2026, 1351, 144240.
14. Hasan MM, Fatema Tuj Z. Valorized oxalic acid treated onion peel (*Allium cepa*) and jute stick (*Chorchorus olitorius*) wastes for dye removal from tannery effluents. *Desalin. Water Treat.*, 2024, 319, 100554.
15. Moatamed Sabzevar A, Ahmadpour A, Ghahramaninezhad M, Arami-Niya A. Tuning cross-linker type in the fabrication of beta-cyclodextrin/magnetic lignin adsorbents: Comparative study of cationic dye adsorption performance. *Env. Technol. Innovation*, 2025, 40, 104507.
16. Kareem A, Alrazak NA, Aljebori KH, Aljeboree AM, Algboory HL, Alkaim AF. Removal of methylene blue dye from aqueous solutions by using activated carbon/urea formaldehyde composite resin as an adsorbent. *Int. J. Chem. Sci.*, 2016, 14(2), 635-648.
17. Ravichandran B, Zhang W, Liu H, Khotseng L, Su H. Graphitic carbon nitride (g-C_3N_4) in fuel cells: A comprehensive review of synthesis, functionalization, and multifaceted electrocatalytic roles. *J. Alloys Compd.*, 2025, 1042, 183989.
18. Eti IA, Khatun M, Khatun MA, Rahman MO, Anis-Ul-Haque KM, Alam MJ. Removal of dye from wastewater using a novel composite film incorporating nanocellulose. *Adv. Polym. Technol.*, 2023, 2023(1), 4431941.
19. Bijari M, Shahbazi A. Flow-driven engineering of g-C_3N_4 nanosheet for additive-free, one-step, and sustainable synthesis of high-efficiency photocatalysts. *Mater. Today Commun.*, 2025, 114208.
20. Etemadi H, Afsharkia S, Zinatloo-Ajabshir S, Shokri E. Effect of alumina nanoparticles on the antifouling properties of polycarbonate-polyurethane blend ultrafiltration membrane for water treatment. *Polym. Eng. Sci.*, 2021, 61(9), 2364-2375.
21. Fatimah I, Fadillah G, Sahroni I, Kamari A, Sagadevan S, Doong R-A. Nanoflower-like composites of ZnO/SiO_2 synthesized using bamboo leaves ash as reusable photocatalyst. *Arabian J. Chem.*, 2021, 14(3), 102973.
22. Luo Y, Zhu Y, Han Y, Ye H, Liu R, Lan Y, Xue M, Xie X, Yu S, Zhang L.

$g-C_3N_4$-based photocatalysts for organic pollutant removal: A critical review. *Carbon Res.*, 2023, 2(1), 14.
23. Esmaeili H, Foroutan R. Adsorptive behavior of methylene blue onto sawdust of sour lemon, date palm, and eucalyptus as agricultural wastes. *J. Dispersion Sci. Technol.*, 2018, 40(7), 990-999. https://doi.org/910.1080/01932691.0193 2018.01489828
24. Modwi A, Elamin MR, Idriss H, Elamin NY, Adam FA, Albadri AE, Abdulkhair BY. Excellent adsorption of dyes via $MgTiO_3$@$g-C_3N_4$ nanohybrid: Construction, description and adsorption mechanism. *Inorganics*, 2022, 10(11), 210.
25. Aljeboree AM, Alkaim AF. Comparative removal of three textile dyes from aqueous solutions by adsorption: As a model (corn-cob source waste) of plants role in environmental enhancement. *Plant Arch.*, 2019, 19(1), 1613-1620.
26. Hayeeye F, Sattar M. Removal of crystal violet in aqueous solution by activated carbon from the pericarp of rubber fruit and bagasse: Kinetics, thermodynamics and adsorption studies. *Desalin. Water Treat.*, 2020, 202 420-434.
27. Elelu SA, Adebayo GB, Abdus-Salam N, Iriowen EM. Preparation and characterization of adsorbents from physic nut plant (*Jatropha curcas* L). *Chemist*, 2018, 91(2) 42-49.
28. Elamin MR, Ben Aissa MA, Al-Ayed AS, Modwi A. Adsorption performance of Congo red and malachite green in binary system using Co_3O_4 and Fe_2O_3 co-doped $g-C_3N_4$. *Inorg. Chem. Commun.*, 2026, 186, 116258.
29. Zhang H, Huang J, Zhong M, He F, Dong N, Su B, Lei Z. S-scheme $g-C_3N_4/Bi_2MoO_6$ heterojunction for enhanced adsorption and visible-light photocatalytic removal of antibiotics: Mechanistic insights and transformation pathways. *J. Photochem. Photobiol., A*, 2026, 476, 117098.
30. Zubair M, Manzar MS, Mu'azu ND, Anil I, Blaisi NI, Al-Harthi MA. Functionalized MgAl-layered hydroxide intercalated date-palm biochar for enhanced uptake of cationic dye: Kinetics, isotherm and thermodynamic studies. *Appl. Clay Sci.*, 2020, 190, 105587.
31. Zoya Z, Aisha A, Elham SA. Adsorption of methyl red on biogenic Ag@Fe nanocomposite adsorbent: Isotherms, kinetics and mechanisms. *J. Mol. Liq.*, 2019, 283, 287-298. https://doi.org/210.1016/j.molliq.2019.1 003.1030
32. Garg R, Gupta R, Bansal A. Synthesis of $g-C_3N_4/ZnO$ nanocomposite for photocatalytic degradation of a refractory organic endocrine disrupter. *Mater. Today: Proc.*, 2021, 44, 855-859.
33. Zinatloo-Ajabshir S, Mortazavi-Derazkola S, Salavati-Niasari M. $Nd_2O_3-SiO_2$ nanocomposites: A simple sonochemical preparation, characterization and photocatalytic activity. *Ultrason. Sonochem.*, 2018, 42, 171-182.
34. Chabib L, Miskam M, Kaus NHM, Shafie MH, Hamid M, Saragi IR, Isnaeni I, Amilia D, Dalimunthe IB, Wijoyo H. Optimization of $g-C_3N_4$ nanoparticles on structural, morphological, and optical properties as organic pollutants adsorbent in glycerin. *Case Stud. Chem. Env. Eng.*, 2025, 11, 101057.
35. Zinatloo-Ajabshir S, Ahmadi-Zeidabadi M, Amiri M, Sharifianjazi F. Innovative sono-synthesis of cerium dioxide nanomaterials using mentha extract

with efficient activity for cancer therapy application. *Results Eng.*, 2024, 23, 102720. https://doi.org/102710.101016/j.rineng.102024.102720
36. Zhokh A, Strizhak P. Crossover between Fickian and non-Fickian diffusion in a system with hierarchy. *Microporous Mesoporous Mater.*, 2019, 282, 22-28. https://doi.org/10.1016/j.micromeso.2019.1003.1016
37. Zheng X, Li X, Li J, Wang L, Jin W, Liu J, Pei Y, Tang K. Efficient removal of anionic dye (Congo red) by dialdehyde microfibrillated cellulose/chitosan composite film with significantly improved stability in dye solution. *Int. J. Biol. Macromol.*, 2018, 107, 283-289.
38. Sabah NA, Aljeboree A, Jasim KK. Eco-friendly and low-cost hydrogel nanocomposite to efficiently remove textile dye from aqueous solution: Thermodynamics and regeneration study. *J. Nanostruct.*, 2025, 15(1), 210-218.
39. Zhao Y, Zhou H, Song M, Xu Z, Sun Z, Xu Q, Chen Y, Liao X. Interface engineering of Ti-MOFs: Adsorption of anionic, cationic and neutral dyes in wastewater. *J. Mol. Struct.*, 2023, 1283, 135268.
40. Zhang L, Sellaoui L, Franco D, Dotto GL, Bajahzar A, Belmabrouk H, Bonilla-Petriciolet A, Oliveira MLS, Li Z. Adsorption of dyes Brilliant Blue, sunset yellow and tartrazine from aqueous solution on chitosan: Analytical interpretation via multilayer statistical physics model. *Chem. Eng. J.*, 2020, 382, 122952.
41. Zainul R, Basem A, Nemah AK, Kumar R, Kumar R, Sharma R, Aljeboree AM, Chahar M, Elmasry Y. BP-biphenylene monolayers: A promising anode material for high-performance magnesium-ion batteries. *Inorg. Chem. Commun.*, 2024, 168.
42. Li K, Chen M, Chen L, Zhao S, Xue W, Han Z, Han Y. Synthesis of g-C_3N_4 derived from different precursors for photodegradation of sulfamethazine under visible light. *Processes*, 2023, 11(2), 528.
43. Hameed BH. Equilibrium and kinetic studies of methyl violet sorption by agricultural waste. *J. Hazard. Mater.*, 2008, 154, 204-212.
44. Hadi ZA, Aljeboree AM, Alkaim AF. Adsorption of a cationic dye from aqueous solutions by using waste glass materials: Isotherm and thermodynamic studies. *Int. J. Chem. Sci.*, 2014, 12(4), 1273-1288.
45. Hameed Mahmood Z, Riadi Y, Hammoodi HA, Alkaim AF, Fakri Mustafa Y. Magnetic nanoparticles supported copper nanocomposite: A highly active nanocatalyst for synthesis of benzothiazoles and polyhydroquinolines. *Polycyclic Aromat. Compd.*, 2023, 43(4), 3687-3705.
46. Long R, Yu Z, Tan Q, Feng X, Zhu X, Li X, Wang P. Ti_3C_2 MXene/NH2-MIL-88B (Fe): Research on the adsorption kinetics and photocatalytic performance of an efficient integrated photocatalytic adsorbent. *Appl. Surf. Sci.*, 2021, 570, 151244.
47. Rahul null, Jindal R. Efficient removal of toxic dyes malachite green and fuchsin acid from aqueous solutions using Pullulan/CMC hydrogel. *Polymer*, 2024, 307, 127203. https://doi.org/127210.121016/j.polymer.122024.127203
48. Aljeboree AM, Abbas AS. Removal of pharmaceutical (paracetamol) by using CNT/ TiO_2 nanoparticles. *J. Global Pharma Technol.*, 2019, 11(1): 199-

205.
49. Sharma AK, Priya null, Kaith BS, Sharma N, Bhatia JK, Tanwar V, Panchal S, Bajaj S. Selective removal of cationic dyes using response surface methodology optimized gum acacia-sodium alginate blended superadsorbent. *Int. J. Biol. Macromol.*, 2019, 124, 331-345. https://doi.org/310.1016/j.ijbiomac.2018.1011.1213
50. Sharma AK, Dhiman A, Nayak AK, Mishra R, Agrawal G. Environmentally benign approach for the efficient sequestration of methylene blue and Coomassie Brilliant Blue using graphene oxide emended gelatin/خ؛-carrageenan hydrogels. *Int. J. Biol. Macromol.*, 2022, 219, 353-365. https://doi.org/310.1016/j.ijbiomac.2022.1007.1216
51. Serban GV, Iancu VI, Dinu C, Tenea A, Vasilache N, Cristea I, Niculescu M, Ionescu I, Chiriac FL. Removal efficiency and adsorption kinetics of methyl orange from wastewater by commercial activated carbon. *Sustainability*, 2023, 15, 12939. DOI: 10.3390/su151712939
52. Sahmoune MN. Evaluation of thermodynamic parameters for adsorption of heavy metals by green adsorbents. *Env. Chem. Lett.*, 2019, 17(2), 697-704.
53. Boparai HK, Joseph M, O'Carroll DM. Kinetics and thermodynamics of cadmium ion removal by adsorption onto nano zerovalent iron particles. *J. Hazard. Mater.*, 2011, 186(1), 458-465.
54. Bazargan-Lari R, Zafarani HR, Bahrololoom ME, Nemati A. Removal of Cu(II) ions from aqueous solutions by low-cost natural hydroxyapatite/chitosan composite: Equilibrium, kinetic and thermodynamic studies. *J. Taiwan Inst. Chem. Eng.*, 2014, 45(4) 1642-1648.
55. Girish CR. Determination of thermodynamic parameters in adsorption studies: A review. *Chem. Pap.*, 2025, 79(9), 5687-5706.
56. Xue J, Ji M, Lu Y, Pan D, Yang X, Yang X, Xu Z. The impact of chemical properties of the solid–liquid–adsorbate interfaces on the entropy–enthalpy compensation involved in adsorption. *Phys. Chem. Chem. Phys.*, 2024, 26(11), 8704-8715.
57. Shahcheragh SK, Bagheri Mohagheghi MM, Shirpay A. Effect of physical and chemical activation methods on the structure, optical absorbance, band gap and Urbach energy of porous activated carbon. *SN Appl. Sci.*, 2023, 5(12), 313.
58. Alibrahim KA. The adsorption behaviors of industrial dyes by natural mordenite: isotherm, kinetic, thermodynamic, and Box–Behnken design study. *Desalin. Water Treat.*, 2023, 298, 155-173.
59. Junejo R, Shams Jalbani N, Kaya S, Serdaroglu G, Şimşek S, Memon S. Experimental and DFT modeling studies for the adsorptive removal of reactive dyes from wastewater. *Sep. Sci. Technol.*, 2022, 57(3), 339-353.
60. Gutiérrez P, Aldas M, Gavilanes D, Cadena F, Valle V. Corn cob valorization: Synthesis of a polymer based on crystalline cellulose with poly(ethylene glycol) diacrylate and N-vinylcaprolactam. *Cleaner Eng. Technol.*, 2025, 27, 101019.
61. Guerra-Que Z, López-Margalli KS, Urrieta-Saltijeral JM, Silahua-Pavón AA, Martínez-García H, García-Alamilla P, Córdova-Pérez GE, Arévalo-Pérez JC, Torres-Torres JG. Activated carbon synthesised from lignocellulosic cocoa pod husk via alkaline and acid treatment for methylene blue adsorption:

Optimisation by response surface methodology, kinetics, and isotherm modelling. *RSC Adv.*, 2025, 15(55), 47231-47254.

62. Kumari B, Chauhan S, Chauhan GS, Kumar K, Jamwal P, Ranote S. A two-in-one thiosemicarbazide and whole pine needle-based adsorbent for rapid and efficient adsorption of methylene blue dye and mercuric ions. *Env. Sci. Pollut. Res.*, 2024, 31(14), 21591-21609. https://doi.org/21510.21007/s11356-21024-32446-21593
63. Shubha JP, Kavalli K, Adil SF, Assal ME, Hatshan MR, Dubasi N. Facile green synthesis of semiconductive ZnO nanoparticles for photocatalytic degradation of dyes from the textile industry: A kinetic approach. *J. King Saud Univ., Sci.*, 2022, 34(5), 102047.
64. Sharma S, Sharma G, Kumar A, AlGarni TS, Naushad M, Alothman ZA, Stadler FJ. Adsorption of cationic dyes onto carrageenan and itaconic acid-based superabsorbent hydrogel: Synthesis, characterization and isotherm analysis. *J. Hazard. Mater.*, 2021, 421, 126729. https://doi.org/126710.121016/j.jhazmat.122021.126729